ACS APPLIED ELECTRONIC MATERIALS

pubs.acs.org/acsaelm Article

Ammonium Salt Assisted Crystallization for High Performance Two-Dimensional Lead-Free Perovskite Photodetector

Tao Huang, Ruiyan Li, Xuhang Chen, Ying Li, Yulei Chang, Wei Li,* and Weili Yu*

Cite This: ACS Appl. Electron. Mater. 2023, 5, 2169−2177 Read Online

ACCESS | Metrics & More | Article Recommendations | Supporting Information

ABSTRACT: Two-dimensional Ruddlesden−Popper lead-free perovskites show promising prospects for application in optoelectronic devices due to their tunable optoelectronic properties and environmental friendliness. However, their carrier mobility and stability are limited by the crystal morphology and lattice direction, which hinder the improvement of their optoelectronic device performance. Here, we introduce a convenient ammonium assistance method to improve the crystallinity and lattice orientation of 2D perovskite films, through which carrier mobility and stability of 2D perovskites can be significantly improved. Oriented crystals, increased grain size, and improved crystal quality contribute to the high performance of lateral photodetectors. The champion device exhibits high Responsivity, External Quantum Efficiency, and Detectivity (938 A/W, 34714%, and 3.70 × 10^{14} Jones, respectively), as well as outstanding stability. This work reveals the potential of ammonium assistance 2D perovskite in developing high-performance and stable optoelectronic devices.

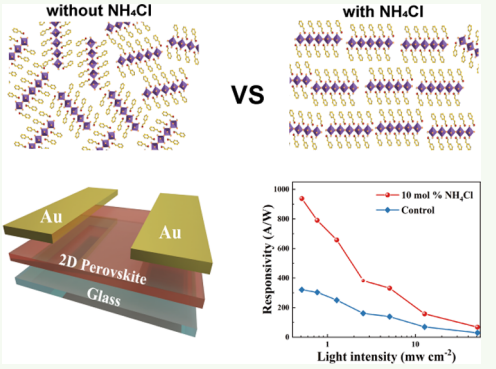

KEYWORDS: *2D perovskite, lead-free perovskite, ammonium chloride, crystallization, photodetector*

INTRODUCTION

In recent years, metal halide perovskites (MHP) have become a promising semiconductor for optoelectronic devices due to their superior photoelectric properties, including high absorption coefficient, large carrier mobility, and tunable band gap.[1−4] Nevertheless, the vulnerable tolerance to moisture and oxygen in the environment seriously restricts their further development and practical applications. 2D Ruddlesden−Popper perovskite has been concerned as a potential candidate for environmentally stable optoelectronics devices. Its structure can be described as the formula $A_2A'_{n-1}B_nX_{3n+1}$, where A is a large organic monovalent cation (e.g., Phenethylammonium (PEA^+)), A′ is a short-chain monovalent cation (e.g., Methylammonium (MA^+)), B is a divalent ion such as Pb^{2+} and Sn^{2+}, anion X is a halide, and n represents the layer number of octahedral monolayers between the organic spacer A′ layers.[5,6] Compared with their 3D counterparts, the unique hydrophobic A′ layer structure of 2D perovskite effectively prevents the moist erosion to the octahedral layer, thus enhancing the long-term stability on one hand,[7] while, on the other hand, it forms multiple quantum wells owing to the A′ layers' strong insulating character, which leads to dielectric confinement because of large exciton-binding energy and high permittivity, thus inhibiting charge transport between the two adjacent conducting layers[8] and further hindering the improvement in device performance.[9,10]

To achieve highly efficient devices, various approaches have been explored. One approach to solve this problem involves tuning the lattice structures by increasing the number of inorganic layers (n value);[11,12] the performances are improved but in exchange for a severe stability decline. An alternative approach to the problem is improving crystallinity and morphology to guarantee the efficient collection of carriers.[13] Substrate treatment,[14] multilayer engineering,[15] and hot-casting deposition[5] methods have been developed, and a range of 2D perovskite thin films have been fabricated with preferred crystallinity. The corresponding photodetectors display improved Responsivity.[16,17] However, these methods increase the complexity of the process, limits the yield, and offers limited performance gains. Therefore, it is urgent to explore an efficient, convenient, and universal method to improve the crystallinity and morphology of 2D perovskites.[18]

Beyond crystallinity and morphology, the choice of divalent cation is also a key issue for developing desirable devices. It is reported that lead would restrict the regulation ability of 2D perovskite devices due to its strong insulation;[19,20] meanwhile, the potential risk of environmental pollution caused by lead

Received: January 15, 2023
Accepted: March 29, 2023
Published: April 10, 2023

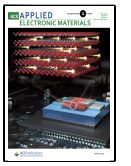

https://doi.org/10.1021/acsaelm.3c00058
ACS Appl. Electron. Mater. 2023, 5, 2169−2177

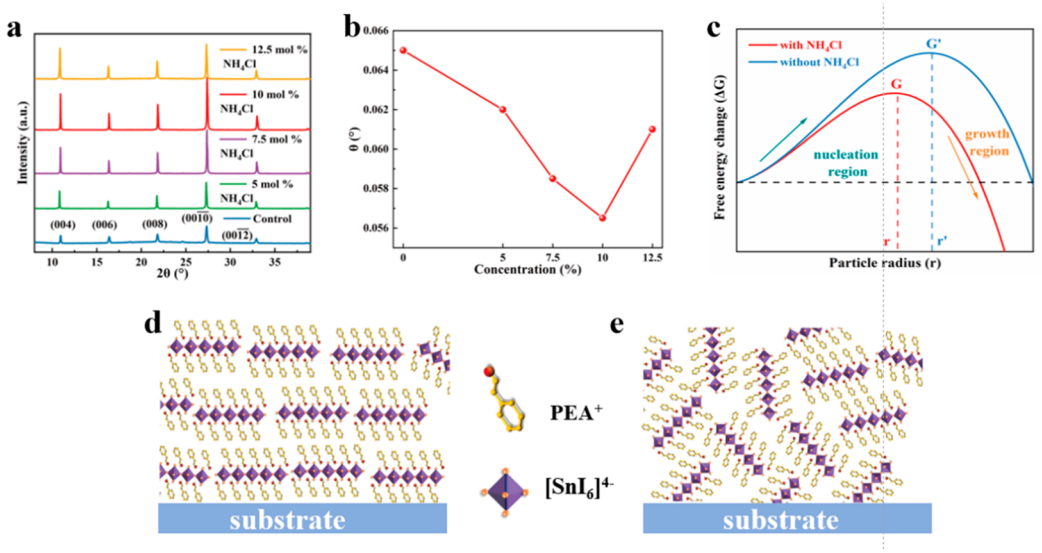

Figure 1. (a) XRD patterns of 2D perovskite films with different concentrations NH_4Cl additives. (b) FWHM in the (004) crystal plane versus NH_4Cl concentration. (c) Gibbs free energy as a function of r for perovskite with or without NH_4Cl. The crystallization of perovskite can only be triggered after overcoming the G' and obtaining a nucleus exceeding the r'. Schematic diagram of 2D perovskite crystal stacking pattern for (d) NACF and (e) control samples.

leakage impedes its practical application. To resolve this problem, tin-based perovskite is expected to achieve a balance in performance and environmental protection,[21] although Sn^{2+} is easily oxidized and causes insufficient device stability.[22,23]

Herein, we introduce ammonium chloride (NH_4Cl) as an additive in the tin-based perovskite precursor solution to regulate the crystallization thermodynamics and to assist 2D perovskite growth in the spin coating process. The grain size and surface flatness of NH_4Cl-assisted crystalline film (NACF) were significantly improved. The high-quality thin film endows the photodetector with a peak Responsivity of 938 A W^{1-}, a high External Quantum Efficiency (EQE) of 4.99×10^6%, and a Detectivity as much as 3.70×10^{14} cm $Hz^{1/2}$ W^{1-} (Jones), which is superior to that reported for 2D perovskite photodetectors. In addition, the device maintains 92.4% of the initial performance after 40 days. Our research provides an efficient and convenient method for improving the crystallinity and morphology of 2D perovskite and broadening their application prospects.

RESULTS AND DISCUSSION

The 2D perovskite precursor solution of the control group was prepared by dissolving phenethylammonium iodide (PEAI) and tin(II) iodide at a molar ratio of 2:1 in *N*,*N*-dimethylformamide (DMF) solvent. Then a gradient concentration of NH_4Cl from 5 mol % to 12.5 mol % was added into a precursor solution to adjust the crystallization process. During the annealing process, part of NH_4Cl will assist the formation of the perovskite skeleton, while the other part will volatilize. The films were fabricated on the hydrophilic glass substrate through a one-step spin-coating process. The hydrophilicity of the glass substrate was achieved by oxygen plasma cleaning (Figure S1), which was beneficial to the film uniformity.[24,25] Afterward, 700 nm highly oriented 2D perovskite films were prepared.

To assess the effect of NH_4Cl on crystallinity, the X-ray diffraction (XRD) measurements were performed. As presented in Figure 1a, all sample films exhibit intense, sharp, and well-defined diffraction peaks, repeated periodically without other miscellaneous peaks, signature of the (00h) (h = 4, 6, 8. . .) planes in the layered $(PEA)_2SnI_4$ crystalline structure.[7,26] XRD results confirm that the films are preferentially parallel to the substrate with the assistance of NH_4Cl.[22,27] The intensity of diffraction peak increases by about 70 times when the NH_4Cl concentration increases from 0 to 10 mol %, which verifies the improved crystallization due to NH_4Cl. It is worth mentioning that when the NH_4Cl concentration rises to 12.5 mol %, the crystallinity of the film decreases instead. The reason may be due to the fact that NH_4Cl is unable to become volatile completely, thus affecting the crystallinity process of 2D perovskite.[28,29] We characterized the energy dispersive X-ray spectroscopy (EDS) for verification. The 10 mol % film exhibited no residual chlorine, while scattered chlorine was found in 12.5 mol % film for comparison, as shown in Figure S2. The relationship between the full width at half-maximum (FWHM) of the (004) crystal plane and NH_4Cl concentration was presented in Figure 1b. The diffraction angle θ ranges from ~0.065° to ~0.056° when the concentration increases from 0 to 10 mol %, and then falls back to ~0.061° for 12.5 mol %. According to the Scherrer equation, the FWHM is inversely proportional to grain size, which indicates that the average grain size of the 2D perovskite film increases and then decreases with increasing NH_4Cl correspondingly.[29,30] These results suggest that NH_4Cl can efficiently construct highly oriented crystal structures and enlarge the grain size of 2D perovskite. Other ammonium salts have also been tried as an additives, such as NH_4Br and NH_4I. However, several peaks are missing in the XRD patterns, as shown in Figure S3, which may be attributed to the residual of bromine and iodine during spin coating.

The crystallization process contains two steps, nucleation and growth.[31] It can be described by Gibbs free energy curves using equations:[32]

$$G = \frac{4}{27}\frac{(\Sigma_i \eta_i \Gamma_i)^3}{(\mu_2 - \mu_1)^2} \quad (1)$$

https://doi.org/10.1021/acsaelm.3c00058
ACS Appl. Electron. Mater. 2023, 5, 2169−2177

$$r = -\frac{8}{27}\left\{\frac{\Sigma_i \eta_i \Gamma_i}{\mu_2 - \mu_1}\right\}^3 \quad (2)$$

where G is the Gibbs free energy, r is the grain size, η_i represents the shape factor for the ith, Γ_i represents the interfacial free energy per unit interfacial area for the ith area, and μ_1 and μ_2 represent the respective chemical potentials of the bulk amorphous and crystalline phases.

The nucleation rate of uniform nucleation refers to the number of nuclei formed per unit volume of metastable phase solution per unit time:[33]

$$I = B \exp\left(-\frac{\Delta G_c}{kT}\right) \quad (3)$$

where B is the proportional constant, which depends on the kinetic factors of growth, ΔG_c is the work required to form the critical nucleus, k is the Boltzmann constant, and T is the temperature. It can be found that the crystal nucleation rate is negatively correlated with the critical nucleation barrier.

Figure 1c presents NACF and control sample's Gibbs free energy curves, which indicates that the crystal growth needs to surmount the nucleation barrier until spontaneous growth.[34] Due to the NH_4Cl assistance, the underlying perovskite nucleation is more rapid and flat. And the faster and smoother nucleation process in NACF means that the nucleation shape is more regular with the same interfacial binding energy, resulting in a lower η_i and thus a lower nucleation barrier.[34,35]

Previous works have shed light on the crystallization mechanism of 2D perovskite.[36,37] The calculations of adsorption energies for NH_4^+ show that it has strong binding ability with the PEA molecule, which may account for the unique advantage of NH_4^+ in regulating the 2D perovskite orientation.[29] Ascribing to the presence of cations in the insulating spacer, the vertical transport of carriers is suppressed, which makes the carrier transport confined in the SnI_6^{4-} layer of 2D perovskite films.[38,39] Figure 1d and Figure 1e illustrate the schematic diagram of crystal stacking with or without NH_4Cl assistance. NH_4Cl can act as a linker to connect the substrate and the bottom PEA molecule, which impacts 2D perovskite highly oriented parallel to the substrate and facilitates the carriers' lateral transport.[40,41] On the contrary, the stacking orientation of 2D perovskites shows more randomness in the absence of NH_4Cl assistance.

The crystallization rates of NACF and control sample are as shown in Figure 2a, b. Due to the NH_4Cl assistance, the underlying 2D perovskite shows a faster nucleation rate, indicating rapid passage through the nucleation barrier. Beyond that, according to the LaMer curve,[42] with the assistance of NH_4Cl, the solution will be consumed rapidly, thus inhibiting random nucleation. The reduction of random nucleation probability further increases the grain size and improves the film flatness, as illustrated in Figure 2a and Figure 2b. Figure 2c and Figure 2d show the scanning electron microscope (SEM) pictures of NACF and control samples. Compared with the obvious fluctuations and fragmentation of control sample, NH_4Cl improves the film flatness of NACF significantly, reduces the nonradiative recombination of carriers, and extends the carrier diffusion distance.[43] Figure 2e and Figure 2f present the atomic force microscope (AFM) images of NACF and control samples. From which, the NACF exhibits low surface fluctuation, and the root-mean-squared (RMS) roughness decreases from 2.76 nm for the control sample to 1.40 nm for the NACF sample. This result further confirms that NH_4Cl can regulate the crystallization of 2D perovskite thin films.

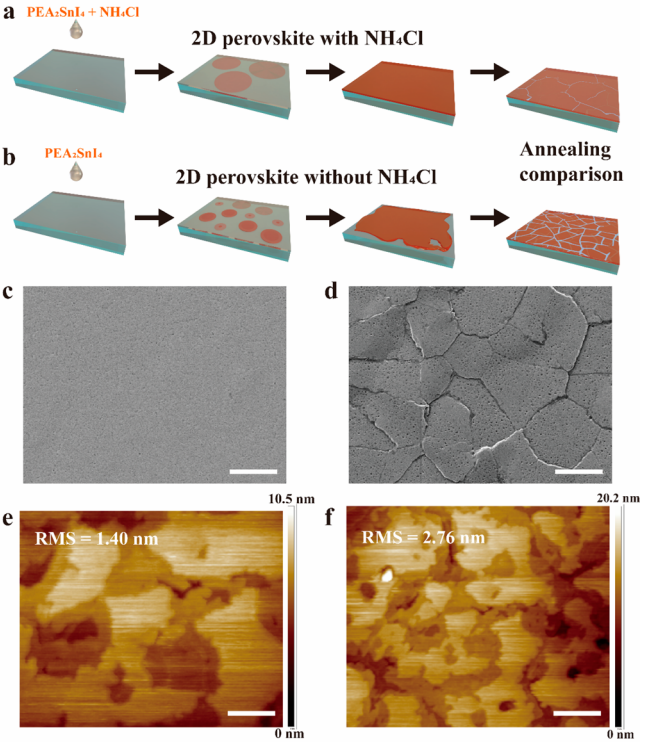

Figure 2. Schematic diagram of 2D perovskite growth (a) with and (b) without NH_4Cl assistance. SEM images of (c) NACF and (d) control samples. Scale bar: 5 μm. AFM images of (e) NACF and (f) control samples. Scar bar: 500 nm.

To further understand the influence of NH_4Cl on 2D perovskite properties, we conducted optical and electrical characterizations. The 80 nm Au electrodes with a 25 μm width channel were deposited evenly on the crystal surface by thermal evaporation method, as shown in Figure S4. Figure 3a shows the $J-V$ characteristics of devices at room temperature, which indicates that the carrier mobility has been enhanced by more than 15 times, benefiting from the highly efficient charge transport because of the well aligned crystallinity.[44] The UV−vis absorption spectra reveal that both samples exhibit similar optical band gaps and sharp exciton peaks, indicating the addition of NH_4Cl does not change the shape (the embodiment of band structure and exciton characteristics) of the films (Figure 3b). However, the NACF sample shows improved absorbance, which is believed to be conducive to optoelectronic device applications. Figure S5 measured the UV−vis absorption spectra of NACF samples with varying NH_4Cl concentrations, and similar optical band gaps and sharp exciton peaks can be observed for all samples.

In order to further explore the carrier recombination transition, photoluminescence (PL) spectroscopy was conducted under the same power excitation of 473 nm. The peaks at 625 nm are observed for both NACF and control samples, as shown in Figure 3c. The NACF generates significantly enhanced PL, indicating that the improved film morphology effectively reduces the occurrence of nonradiative recombination.[45] The PL spectra of other concentrations with consistent trend are shown in Figure S6a, and the highest PL intensity was achieved when the concentration of NH_4Cl is 7.5 mol %.

https://doi.org/10.1021/acsaelm.3c00058
ACS Appl. Electron. Mater. 2023, 5, 2169−2177

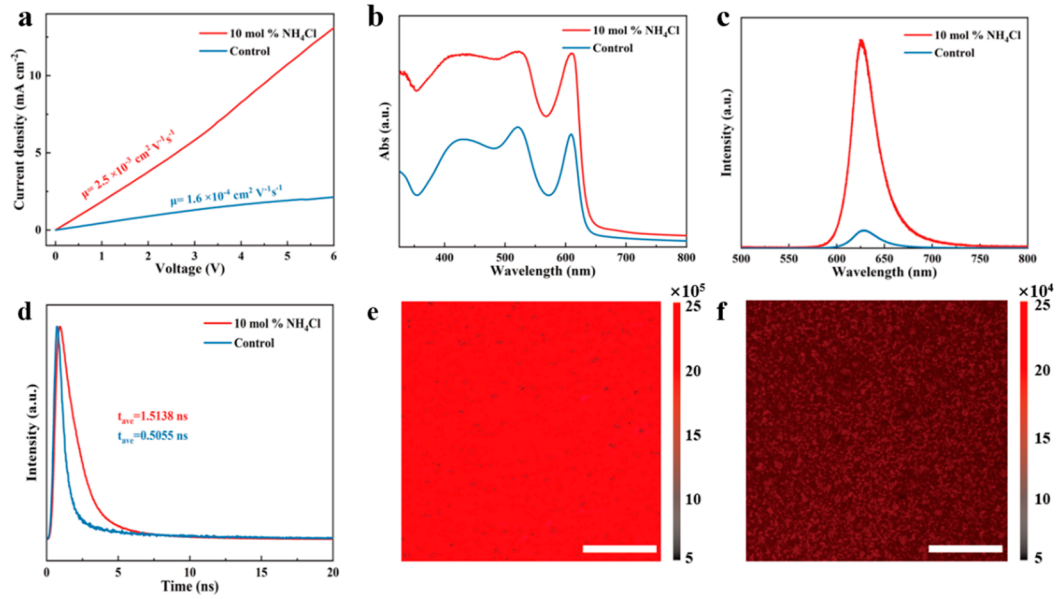

Figure 3. (a) $J-V$ curves, (b) UV−vis absorption, (c) photoluminescence spectra, and (d) TRPL spectra of NACF (10 mol % NH_4Cl) and control samples, respectively. PL mapping for the (e) NACF (10 mol % NH_4Cl) and (f) control 2D perovskite samples. Scar bar: 200 μm.

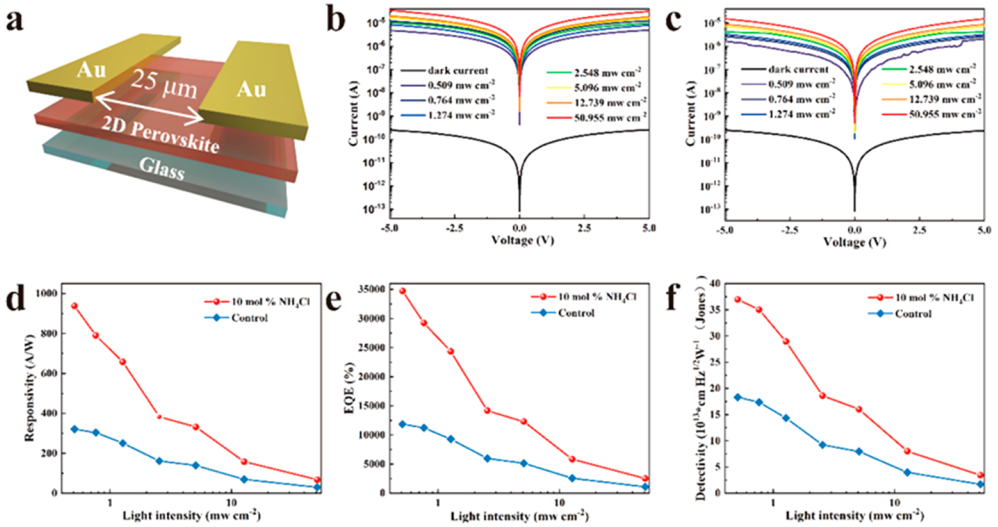

Figure 4. (a) Schematic illustration of the 2D perovskite photodetector. The $I-V$ curves of the 2D perovskite film (b) NACF and (c) control samples in dark and under 532 nm light illumination with varying light intensities. (d) Responsivity, (e) EQE, and (f) Detectivity as a function of incident light intensity for 2D perovskite film photodetectors.

Then we monitored the time-resolved photoluminescence (TRPL) of all samples to further explore the carrier transport modulated mechanism. According to the biexponential fitting, the average lifetimes are calculated to be 1.5138 and 0.5055 ns for NACF (10 mol %) and control samples, respectively[46,47] (Figure 3d). For other concentrations, the average lifetime are calculated to be 1.0527 ns, 1.1520 ns, and 1.0781 ns, respectively, as shown in Figure S6b. The details of fitting parameters are shown in Table S1, which confirms that the enhanced charge transfer is due to NH_4Cl assistance (10 mol % for optimal). Figure 3e and Figure 3f show the PL mapping of both NACF and control samples. A more homogeneous PL distribution and a higher integrated intensity were detected for NACF. The optical and electrical characterizations further confirm the optimization effect of NH_4Cl on 2D perovskite thin films.

To apply these films for optoelectronic detection, a lateral device configuration with the device configuration of Au/2D perovskite/Au (Figure S4) is adopted, as shown in Figure 4a. From the $I-V$ curves of different samples under 532 nm stimulation (Figure 4b and Figure 4c), obvious linear and saturated regions can be observed, and notable light response can be detected. The switching ratio of the samples is greater than 1000, exhibiting strong antinoise interference ability. Moreover, through the NH_4Cl assistance, the 2D perovskite photocurrent intensity increases by three times, illustrating suppression of nonradiative recombination and enhancement in carrier transport. To quantify the optoelectronic performance, we calculated the Responsivity (R), which is indicated as a photocurrent generated under the stimulation of unit light intensity in unit area and can be derived by the following formula:[48]

https://doi.org/10.1021/acsaelm.3c00058
ACS Appl. Electron. Mater. 2023, 5, 2169−2177

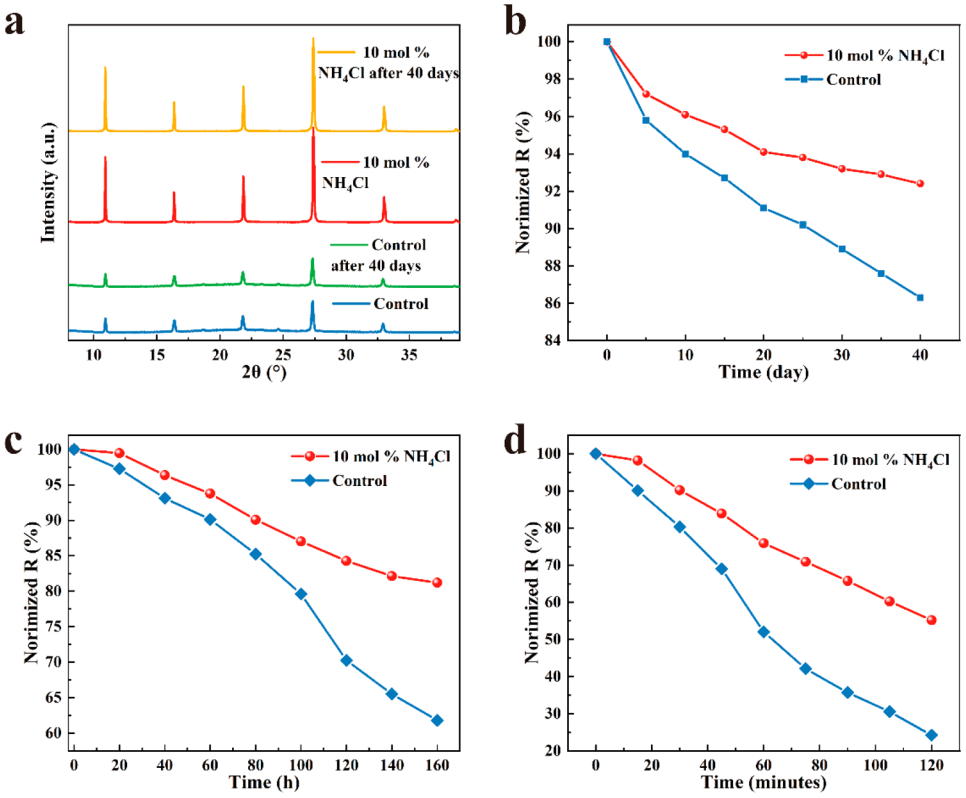

Figure 5. (a) XRD patterns of NACF and control samples stored in a N_2-filled atmosphere at room temperature for different time. (b) Normalized Responsivity variation curves of 2D perovskite films devices stored in a N_2-filled atmosphere at room temperature. (c) Normalized Responsivity variation curves of 2D perovskite films devices stored at 80 °C in a N_2-filled atmosphere. (d) Normalized Responsivity variation curves of 2D perovskite films devices stored at room temperature with RH 60%.

$$R = \frac{I_{light} - I_{dark}}{P_{in}{}^{*}A} \tag{4}$$

where I_{light}, I_{dark}, P_{in}, and A are the photocurrent, dark current, incident optical power density, and effective working area, respectively. According to this equation, the Responsivity as a function of light intensity is calculated and depicted in Figure 4d. The maximum Responsivity of NACF is estimated to be 938 A/W at 0.509 mw/cm^2, which makes a new record in reported 2D perovskite photodetectors (Table S2). For comparison, the control sample shows 320 A/W under the same conditions. The striking contrast reveals that ordered lateral alignment of 2D perovskite is beneficial for enhancing lateral carrier transport. The Responsivity of NACFs with other concentrations are displayed in Figure S7a.

The EQE is the ratio of the number of excitation electrons versus incident photons as below:[49]

$$\mathrm{EQE} = \frac{Rh\nu}{e} \tag{5}$$

where h is Planck's constant, e is the electron charge, and ν is the frequency of light. Figure 4e shows the EQE of different samples, and the changing trend coincides with the Responsivity. An EQE of 34714% is achieved for the NACF (10 mol %) sample, reflecting efficient carrier transport. The EQE of NACFs with other concentrations are displayed in Figure S7b.

Detectivity (D) is another key parameter that characterizes the ability to detect weak light signals under various noises. In our experiment environment, dark current is mainly affected by short noise and thus D is expressed by:[50]

$$D = \frac{R}{\sqrt{2eJ_{dark}{}^{2}}} \tag{6}$$

where J_{dark} is the dark current density of the photodetector. Figure 4f and Figure S7c represent D as a function of light intensity. The peak Detectivity increases from 1.83×10^{14} Jones for the control sample to 3.70×10^{14} Jones for the NACF sample. The enhancement of noise tolerance again illustrates the effect of NH_4Cl assistance on inhibition nonradiative recombination of 2D perovskite. The improvement of the above three key parameters displays the competitive role of NH_4Cl assistance in the fabrication of high-performance 2D perovskite photodetectors. Table S2 summarizes the detailed comparison of performance of 2D perovskite photodetectors in previous reports and in this work. The NH_4Cl assistance method prepared lead-free perovskite shows significant advantages in enhancing performance parameters, thus highlighting the competitiveness of the NH_4Cl assistance strategy in high-performance detector fabrication.

As Sn^{2+} is easily oxidized, the stability is a key issue that restricts the development of tin-based perovskites.[52,53] We have conducted a series of tests to investigate the stability of all 2D perovskite films fabricated. Figure 5a exhibits the XRD patterns of NACF and control samples stored in a N_2-filled glovebox at room temperature. For the NACF sample, after 40 days, the characteristic peak intensity of the sample is reduced slightly and no new peaks are produced, indicating the good

https://doi.org/10.1021/acsaelm.3c00058
ACS Appl. Electron. Mater. 2023, 5, 2169−2177

environmental stability of the NACF. The control sample also shows no new peak, indicating decomposition happens. The normalized Responsivity of both devices is also measured under the same storage conditions, as shown in Figure 5b. The NACF sample maintains 92.4% of initial performance after 40 days, while the corresponding control sample remains at only 86.3%. The reason may lie in the fact that Sn^{2+} oxidization occurs at grain boundaries mostly,[53] and the NH_4Cl assistance increases the grain size and effectively inhibits the occurrence of oxidation.

Then the two films were heated to 80 °C for a heat resistance test, as shown in Figure 5c. The NACF sample retained 81.2% of its initial properties after 160 h. However, the control sample decreased by 39.2%. The migration of iodide ions is the main cause of performance degradation, and iodide ion migration occurs mainly at grain boundaries at high temperature.[54,55] The ordered lattice arrangement effectively increases the grain size and reduces the defect density, thereby improving the thermal stability of the films. For the practical environment test, both devices were stored in air with a relative humidity (RH) of 60%. Figure 5d shows the control sample maintains only 24.2% of initial efficiency after 120 min, while for the NACF sample, the efficiency is nearly unchanged in the initial 30 min and eventually maintained at 55.2% after 120 min. These tests demonstrate that the NH_4Cl assistance is an effective strategy to improve the stability of 2D perovskite films and devices for the practical use of tin-based perovskite.

CONCLUSIONS

In summary, by adding a certain amount of NH_4Cl into the lead-free 2D perovskite precursor solution, highly oriented films parallel to the substrate were fabricated. The 2D perovskite films show regular growth direction, smooth surface morphology, and larger grain size compared to control samples, which is conducive to the transport and radiative recombination of carriers. The champion device exhibits Responsivity, EQE, and Detectivity of 938 A/W, 34714%, and 3.70×10^{14} Jones, respectively. Compared with other 2D photodetectors reported, the device performance has been significantly improved, as well as the stability in a variety of situations. This research provides a practical and convenient method for tuning the crystallization procedures of 2D perovskites and for constructing high-performance photodetectors.

EXPERIMENTAL SECTION

Materials. All the chemicals used in this paper are commercial products which were used as received without further purification. *N*,*N*-Dimethylformamide (DMF, 99%), ammonium iodide (NH_4I, 99%), ammonium bromide (NH_4Br, 99%), and ammonium chloride (NH_4Cl, 99%) were purchased from Aladdin Reagent Ltd. Tin(II) iodide (SnI_2, 99%) and phenylethylammonium iodide (PEAI, 99%) were purchased from Xi'an Polymer Light Technology Corp.

2D Perovskite Solution Preparation. PEAI (1 mmol) and SnI_2 (0.5 mmol) were mixed into 1 mL of DMF to obtain 0.5 mol/L PEA_2SnI_4 precursor solution. Then 5−12.5 mol % NH_4Cl was added into the solutions to get an ammonium salt assisted precursor solution. The solutions were then stirred overnight at 500 rpm before use.

2D Perovskite Film Preparation. The glass substrates were cleaned with deionized water, ethanol, isopropanol, and acetone for 5 min by ultrasound sequentially. After being rinsed with deionized water and dried in a drying box at 100 °C for 5 min, the substrates were processed with UV−O_3 for 3 min to make the substrate hydrophilic.[56] Then 60 μL of PEA_2SnI_4 were dropped onto the glass substrate (1 × 1 cm^2) and spin-coated at 4000 rpm for 40 s. Afterward, the films were transferred onto a hot plate and annealed at 100 °C for 10 min. The spin-coating and annealing processes were completed in a N_2-filled glovebox.

Characterization. We used a HORIBA Scientific Raman spectrometer with 0.255 mW cm^{-2} laser intensity at 473 nm to measure the PL spectra of PEA_2SnI_4 films in air at room temperature. We used a Cary 5000 spectrophotometer from Agilent Company to measure UV−vis the absorption spectra of PEA_2SnI_4 films. The thickness of the films was performed on a Keyence laser confocal microscope (VK-X1000). The X-ray diffraction was characterized by Bruker D8 Focus. The SEM and EDS were characterized by Zeiss Auriga-45-06. The AFM images were characterized by Bruker Dimension Icon.

Photodetectors Fabrication. To fabricate PEA_2SnI_4 lateral photodetectors, we used a thermal evaporation method to deposit 80 nm Au electrodes with a 25 μm channel length on the films.[56] We used a Keithley 4200A Semiconductor Parametric Analyzer (Tektronix) with a C-100 probe station from TPSi-Company to measure the *I*−*V* curves at room temperature in air. And the devices' photoresponse characteristics were measured under a 532 nm laser with tunable light intensity from 0.5095 mW cm^{-2} to 50.95 mW cm^{-2}.

ASSOCIATED CONTENT

Supporting Information

The Supporting Information is available free of charge at https://pubs.acs.org/doi/10.1021/acsaelm.3c00058.

Hydrophobicity of substrates, EDS mapping of PEA_2SnI_4 films, XRD patterns, the optical image of Au electrodes, UV−vis absorption spectra, PL and TRPL spectra, perovskite photodetector performance as a function of incident light intensity, table on TRPL fitting data of 2D perovskite films, and table on performance comparison of 2D perovskite-based photodetectors. (PDF)

AUTHOR INFORMATION

Corresponding Authors

Wei Li − *GPL Photonic Laboratory, State Key Laboratory of Luminescence and Applications, Changchun Institute of Optics, Fine Mechanics and Physics, Chinese Academy of Science, Changchun 130033, P. R. China; University of Chinese Academy of Sciences, Beijing 100049, P. R. China;* orcid.org/0000-0002-2227-9431; Email: weili1@ciomp.ac.cn

Weili Yu − *GPL Photonic Laboratory, State Key Laboratory of Luminescence and Applications, Changchun Institute of Optics, Fine Mechanics and Physics, Chinese Academy of Science, Changchun 130033, P. R. China; University of Chinese Academy of Sciences, Beijing 100049, P. R. China;* orcid.org/0000-0001-5075-9638; Email: weili.yu@ciomp.ac.cn

Authors

Tao Huang − *GPL Photonic Laboratory, State Key Laboratory of Luminescence and Applications, Changchun Institute of Optics, Fine Mechanics and Physics, Chinese Academy of Science, Changchun 130033, P. R. China; University of Chinese Academy of Sciences, Beijing 100049, P. R. China*

Ruiyan Li − *GPL Photonic Laboratory, State Key Laboratory of Luminescence and Applications, Changchun Institute of Optics, Fine Mechanics and Physics, Chinese Academy of*

https://doi.org/10.1021/acsaelm.3c00058
ACS Appl. Electron. Mater. 2023, 5, 2169−2177

Science, Changchun 130033, P. R. China; University of Chinese Academy of Sciences, Beijing 100049, P. R. China

Xuhang Chen − *GPL Photonic Laboratory, State Key Laboratory of Luminescence and Applications, Changchun Institute of Optics, Fine Mechanics and Physics, Chinese Academy of Science, Changchun 130033, P. R. China; University of Chinese Academy of Sciences, Beijing 100049, P. R. China*

Ying Li − *GPL Photonic Laboratory, State Key Laboratory of Luminescence and Applications, Changchun Institute of Optics, Fine Mechanics and Physics, Chinese Academy of Science, Changchun 130033, P. R. China; University of Chinese Academy of Sciences, Beijing 100049, P. R. China*

Yulei Chang − *University of Chinese Academy of Sciences, Beijing 100049, P. R. China; State Key Laboratory of Luminescence and Applications, Changchun Institute of Optics, Fine Mechanics and Physics, Chinese Academy of Science, Changchun 130033, P. R. China;* orcid.org/0000-0001-7223-1797

Complete contact information is available at: https://pubs.acs.org/10.1021/acsaelm.3c00058

Author Contributions

T.H. and W.Y. conceived the project and designed the experiments. W.Y. designed the device schematic and structure. T.H. fabricated the perovskite samples and conducted the SEM, EDS, optical, XRD, and absorption measurements. Y.C. conducted the PL mapping measurements and analysis. T.H. and R.L. performed the TRPL measurement and analyzed the results. T.H., X.C., and Y.L. performed the PL characterization and analyzed the results. T.H. and R.L. conducted the laser confocal microscopy measurements. W.L. and W.Y. supervised the project. T.H. and W.Y. wrote the manuscript. All authors discussed and commented on the manuscript.

Notes

The authors declare no competing financial interest.

■ ACKNOWLEDGMENTS

This work was supported by the National Natural Science Foundation of China (NSFC, 62134009, 62121005) and Natural Science Foundation of Jilin Province (20220101-203JC).

■ REFERENCES

(1) Zhao, Y.; Ma, F.; Qu, Z.; Yu, S.; Shen, T.; Deng, H.-X.; Chu, X.; Peng, X.; Yuan, Y.; Zhang, X.; You, J. Inactive $(PbI_2)_2RbCl$ stabilizes perovskite films for efficient solar cells. *Science* **2022**, *377* (6605), 531−534.

(2) Kong, W.; Wang, S.; Li, F.; Zhao, C.; Xing, J.; Zou, Y.; Yu, Z.; Lin, C.-H.; Shan, Y.; Lai, Y. H.; Dong, Q.; Wu, T.; Yu, W.; Guo, C. Ultrathin perovskite monocrystals boost the solar cell performance. *Adv. Energy Mater.* **2020**, *10* (34), 2000453.

(3) Tan, S.; Huang, T.; Yavuz, I.; Wang, R.; Yoon, T. W.; Xu, M.; Xing, Q.; Park, K.; Lee, D.-K.; Chen, C.-H.; Zheng, R.; Yoon, T.; Zhao, Y.; Wang, H.-C.; Meng, D.; Xue, J.; Song, Y. J.; Pan, X.; Park, N.-G.; Lee, J.-W.; Yang, Y. Stability-limiting heterointerfaces of perovskite photovoltaics. *Nature* **2022**, *605* (7909), 268−273.

(4) Xing, J.; Zhao, C.; Zou, Y.; Kong, W.; Yu, Z.; Shan, Y.; Dong, Q.; Zhou, D.; Yu, W.; Guo, C. Modulating the optical and electrical properties of $MAPbBr_3$ single crystals via voltage regulation engineering and application in memristors. *Light Sci. Appl.* **2020**, *9* (1), 111.

(5) Tsai, H.; Nie, W.; Blancon, J.-C.; Stoumpos, C. C.; Asadpour, R.; Harutyunyan, B.; Neukirch, A. J.; Verduzco, R.; Crochet, J. J.; Tretiak, S.; Pedesseau, L.; Even, J.; Alam, M. A.; Gupta, G.; Lou, J.; Ajayan, P. M.; Bedzyk, M. J.; Kanatzidis, M. G.; Mohite, A. D. High-efficiency two-dimensional Ruddlesden-Popper perovskite solar cells. *Nature* **2016**, *536* (7616), 312−316.

(6) Qin, C.; Sandanayaka, A. S. D.; Zhao, C.; Matsushima, T.; Zhang, D.; Fujihara, T.; Adachi, C. Stable room-temperature continuous-wave lasing in quasi-2D perovskite films. *Nature* **2020**, *585* (7823), 53−57.

(7) Kagan, C. R.; Mitzi, D. B.; Dimitrakopoulos, C. D. Organic-Inorganic hybrid materials as semiconducting channels in thin-film field-effect transistors. *Science* **1999**, *286* (5441), 945−947.

(8) Chen, Y.; Sun, Y.; Peng, J.; Tang, J.; Zheng, K.; Liang, Z. 2D Ruddlesden-Popper Perovskites for Optoelectronics. *Adv. Mater.* **2018**, *30* (2), 1703487.

(9) Blancon, J.-C.; Even, J.; Stoumpos, C. C.; Kanatzidis, M. G.; Mohite, A. D. Semiconductor physics of organic-inorganic 2D halide perovskites. *Nat. Nanotechnol.* **2020**, *15* (12), 969−985.

(10) Blancon, J. C.; Stier, A. V.; Tsai, H.; Nie, W.; Stoumpos, C. C.; Traoré, B.; Pedesseau, L.; Kepenekian, M.; Katsutani, F.; Noe, G. T.; Kono, J.; Tretiak, S.; Crooker, S. A.; Katan, C.; Kanatzidis, M. G.; Crochet, J. J.; Even, J.; Mohite, A. D. Scaling law for excitons in 2D perovskite quantum wells. *Nat. Commun.* **2018**, *9* (1), 2254.

(11) Li, N.; Zhu, Z.; Chueh, C.-C.; Liu, H.; Peng, B.; Petrone, A.; Li, X.; Wang, L.; Jen, A. K.-Y. Mixed Cation $FA_xPEA_{1-x}PbI_3$ with Enhanced Phase and Ambient Stability toward High-Performance Perovskite Solar Cells. *Adv. Energy Mater.* **2017**, *7* (1), 1601307.

(12) Zheng, H.; Liu, G.; Zhu, L.; Ye, J.; Zhang, X.; Alsaedi, A.; Hayat, T.; Pan, X.; Dai, S. The Effect of Hydrophobicity of Ammonium Salts on Stability of Quasi-2D Perovskite Materials in Moist Condition. *Adv. Energy Mater.* **2018**, *8* (21), 1800051.

(13) Li, Y.; Wu, J.; Zhang, Y.; Zhang, L.; Zhou, X.; Hu, B.; Jiang, Z.; Zeng, J.; Wang, D.; Liu, Y.; Chen, S.; Liu, Z.; Liu, C.; Wang, X.; Xu, B. Whether organic spacer cations induced 2D/3D or quasi-2D/3D mixed dimensional perovskites? *Chem. Eng. J.* **2022**, *450*, 137887.

(14) Kovaricek, P.; Nadazdy, P.; Pluharova, E.; Brunova, A.; Subair, R.; Vegso, K.; Guerra, V. L. P.; Volochanskyi, O.; Kalbac, M.; Krasnansky, A.; Pandit, P.; Roth, S. V.; Hinderhofer, A.; Majkova, E.; Jergel, M.; Tian, J.; Schreiber, F.; Siffalovic, P. Crystallization of 2D Hybrid organic-inorganic perovskites templated by conductive substrates. *Adv. Funct. Mater.* **2021**, *31* (13), 2009007.

(15) Matsushima, T.; Hwang, S.; Sandanayaka, A. S. D.; Qin, C.; Terakawa, S.; Fujihara, T.; Yahiro, M.; Adachi, C. Solution-processed organic-inorganic perovskite field-Effect Transistors with High Hole mobilities. *Adv. Mater.* **2016**, *28* (46), 10275−10281.

(16) Wang, L.; Xue, Y.; Cui, M.; Huang, Y.; Xu, H.; Qin, C.; Yang, J.; Dai, H.; Yuan, M. A Chiral Reduced-Dimension Perovskite for an Efficient Flexible Circularly Polarized Light Photodetector. *Angew. Chem., Int. Ed.* **2020**, *59* (16), 6442−6450.

(17) Ding, R.; Lyu, Y.; Zhao, Y.; Wu, Z.; Guo, F.; Io, W. F.; Pang, S.-Y.; Mao, J.; Wong, M.-C.; Wong, L. W.; Yan, C.; Yu, J.; Zhao, J.; Li, G.; Hao, J. Revealing photovoltaic behavior in 2D hybrid perovskite ferroelectric single-crystalline microwire arrays for self-powered photodetectors. *Mater. Today Phys.* **2022**, *28*, 100867.

(18) Zhu, Z.; Zhu, C.; Yang, L.; Chen, Q.; Zhang, L.; Dai, J.; Cao, J.; Zeng, S.; Wang, Z.; Wang, Z.; Zhang, W.; Bao, J.; Yang, L.; Yang, Y.; Chen, B.; Yin, C.; Chen, H.; Cao, Y.; Gu, H.; Yan, J.; Wang, N.; Xing, G.; Li, H.; Wang, X.; Li, S.; Liu, Z.; Zhang, H.; Wang, L.; Huang, X.; Huang, W. Room-temperature epitaxial welding of 3D and 2D perovskites. *Nat. Mater.* **2022**, *21* (9), 1042−1049.

(19) Noel, N. K.; Stranks, S. D.; Abate, A.; Wehrenfennig, C.; Guarnera, S.; Haghighirad, A.-A.; Sadhanala, A.; Eperon, G. E.; Pathak, S. K.; Johnston, M. B.; Petrozza, A.; Herz, L. M.; Snaith, H. J. Lead-free organic-inorganic tin halide perovskites for photovoltaic applications. *Energy Environ. Sci.* **2014**, *7* (9), 3061−3068.

(20) Hao, F.; Stoumpos, C. C.; Cao, D. H.; Chang, R. P. H.; Kanatzidis, M. G. Lead-free solid-state organic-inorganic halide perovskite solar cells. *Nat. Photonics* **2014**, *8* (6), 489−494.

(21) Xu, D.; Mai, R.; Jiang, Y.; Chen, C.; Wang, R.; Xu, Z.; Kempa, K.; Zhou, G.; Liu, J.-M.; Gao, J. An internal encapsulating layer for efficient, stable, repairable and low-lead-leakage perovskite solar cells. *Energy Environ. Sci.* **2022**, *15* (9), 3891−3900.
(22) Liu, A.; Zhu, H.; Bai, S.; Reo, Y.; Zou, T.; Kim, M.-G.; Noh, Y.-Y. High-performance inorganic metal halide perovskite transistors. *Nat. Electron.* **2022**, *5* (2), 78−83.
(23) Gao, Y.; Wei, Z.; Yoo, P.; Shi, E.; Zeller, M.; Zhu, C.; Liao, P.; Dou, L. Highly Stable Lead-Free Perovskite Field-Effect Transistors Incorporating Linear π-Conjugated Organic Ligands. *J. Am. Chem. Soc.* **2019**, *141* (39), 15577−15585.
(24) Kong, W.; Zhao, C.; Xing, J.; Zou, Y.; Huang, T.; Li, F.; Yang, J.; Yu, W.; Guo, C. Enhancing Perovskite Solar Cell Performance through Femtosecond Laser Polishing. *Solar RRL* **2020**, *4* (7), 2000189.
(25) Zhao, C.; Chen, C.; Wei, R.; Zou, Y.; Kong, W.; Huang, T.; Yu, Z.; Yang, J.; Li, F.; Han, Y.; Guo, C.; Yu, W. Laser-Assisted Synthesis of Ag2S-Quantum-Dot-in-Perovskite Matrix and Its Application in Broadband Photodetectors. *Adv. Opt. Mater.* **2022**, *10* (1), 2101535.
(26) Blancon, J.-C.; Tsai, H.; Nie, W.; Stoumpos, C. C.; Pedesseau, L.; Katan, C.; Kepenekian, M.; Soe, C. M. M.; Appavoo, K.; Sfeir, M. Y.; Tretiak, S.; Ajayan, P. M.; Kanatzidis, M. G.; Even, J.; Crochet, J. J.; Mohite, A. D. Extremely efficient internal exciton dissociation through edge states in layered 2D perovskites. *Science* **2017**, *355* (6331), 1288−1292.
(27) Guo, L.; Qi, Y.; Yang, Z.; Zhao, L.; Zhang, W.; Wang, X.; Liu, H.; Yan, G.; Wang, S.; Pan, C. 2D Ruddlesden-Popper perovskite ferroelectric film for high-performance, self-powered and ultra-stable UV photodetector boosted by ferro-pyro-phototronic effect and surface passivation. *Nano Energy* **2022**, *102*, 107714.
(28) Rong, Y.; Hou, X.; Hu, Y.; Mei, A.; Liu, L.; Wang, P.; Han, H. Synergy of ammonium chloride and moisture on perovskite crystallization for efficient printable mesoscopic solar cells. *Nat. Commun.* **2017**, *8* (1), 14555.
(29) Yang, Y.; Liu, C.; Mahata, A.; Li, M.; Roldán-Carmona, C.; Ding, Y.; Arain, Z.; Xu, W.; Yang, Y.; Schouwink, P. A.; Züttel, A.; De Angelis, F.; Dai, S.; Nazeeruddin, M. K. Universal approach toward high-efficiency two-dimensional perovskite solar cells via a vertical-rotation process. *Energy Environ. Sci.* **2020**, *13* (9), 3093−3101.
(30) Cao, D. H.; Stoumpos, C. C.; Farha, O. K.; Hupp, J. T.; Kanatzidis, M. G. 2D Homologous Perovskites as Light-Absorbing Materials for Solar Cell Applications. *J. Am. Chem. Soc.* **2015**, *137* (24), 7843−7850.
(31) Xu, Z.; Liu, Z.; Li, N.; Tang, G.; Zheng, G.; Zhu, C.; Chen, Y.; Wang, L.; Huang, Y.; Li, L.; Zhou, N.; Hong, J.; Chen, Q.; Zhou, H. A Thermodynamically Favored Crystal Orientation in Mixed Formamidinium/Methylammonium Perovskite for Efficient Solar Cells. *Adv. Mater.* **2019**, *31* (24), 1900390.
(32) Balluffi, R.; Samuel, M.; Carter, W. *Kinetics of Materials*; John Wiley & Sons, Inc: 2005; pp 459−463.
(33) Venables, J. A.; Spiller, G. D. T.; Hanbucken, M. Nucleation and growth of thin films. *Rep. Prog. Phys.* **1984**, *47* (4), 399.
(34) Ummadisingu, A.; Steier, L.; Seo, J.-Y.; Matsui, T.; Abate, A.; Tress, W.; Grätzel, M. The effect of illumination on the formation of metal halide perovskite films. *Nature* **2017**, *545* (7653), 208−212.
(35) Zhao, Y.; Tan, H.; Yuan, H.; Yang, Z.; Fan, J. Z.; Kim, J.; Voznyy, O.; Gong, X.; Quan, L. N.; Tan, C. S.; Hofkens, J.; Yu, D.; Zhao, Q.; Sargent, E. H. Perovskite seeding growth of formamidinium-lead-iodide-based perovskites for efficient and stable solar cells. *Nat. Commun.* **2018**, *9* (1), 1607.
(36) Qing, J.; Liu, X.-K.; Li, M.; Liu, F.; Yuan, Z.; Tiukalova, E.; Yan, Z.; Duchamp, M.; Chen, S.; Wang, Y.; Bai, S.; Liu, J.-M.; Snaith, H. J.; Lee, C.-S.; Sum, T. C.; Gao, F. Aligned and Graded Type-II Ruddlesden-Popper Perovskite Films for Efficient Solar Cells. *Adv. Energy Mater.* **2018**, *8* (21), 1800185.
(37) Lai, H.; Kan, B.; Liu, T.; Zheng, N.; Xie, Z.; Zhou, T.; Wan, X.; Zhang, X.; Liu, Y.; Chen, Y. Two-Dimensional Ruddlesden-Popper Perovskite with Nanorod-like Morphology for Solar Cells with Efficiency Exceeding 15%. *J. Am. Chem. Soc.* **2018**, *140* (37), 11639−11646.
(38) Li, C.; Wang, H.; Wang, F.; Li, T.; Xu, M.; Wang, H.; Wang, Z.; Zhan, X.; Hu, W.; Shen, L. Ultrafast and broadband photodetectors based on a perovskite/organic bulk heterojunction for large-dynamic-range imaging. *Light-Sci. Appl.* **2020**, *9* (1), 31.
(39) Luo, C.; Zheng, G.; Gao, F.; Wang, X.; Zhao, Y.; Gao, X.; Zhao, Q. Facet orientation tailoring via 2D-seed- induced growth enables highly efficient and stable perovskite solar cells. *Joule* **2022**, *6* (1), 240−257.
(40) Min, L.; Tian, W.; Cao, F.; Guo, J.; Li, L. 2D Ruddlesden-Popper Perovskite with Ordered Phase Distribution for High-Performance Self-Powered Photodetectors. *Adv. Mater.* **2021**, *33* (35), 2101714.
(41) Zhang, L.; Sun, C.; He, T.; Jiang, Y.; Wei, J.; Huang, Y.; Yuan, M. High-performance quasi-2D perovskite light-emitting diodes: from materials to devices. *Light-Sci. Appl.* **2021**, *10* (1), 61.
(42) Yang, W. S.; Park, B.-W.; Jung, E. H.; Jeon, N. J.; Kim, Y. C.; Lee, D. U.; Shin, S. S.; Seo, J.; Kim, E. K.; Noh, J. H.; Seok, S. I. Iodide management in formamidinium-lead-halide based perovskite layers for efficient solar cells. *Science* **2017**, *356* (6345), 1376−1379.
(43) Zeng, L.; Chen, S.; Forberich, K.; Brabec, C. J.; Mai, Y.; Guo, F. Controlling the crystallization dynamics of photovoltaic perovskite layers on larger-area coatings. *Energy Environ. Sci.* **2020**, *13* (12), 4666−4690.
(44) Zhang, D.; Fu, Y.; Zhan, H.; Zhao, C.; Gao, X.; Qin, C.; Wang, L. Suppressing thermal quenching via defect passivation for efficient quasi-2D perovskite light-emitting diodes. *Light-Sci. Appl.* **2022**, *11* (1), 69.
(45) Kong, W.; Zhao, C.; Huang, T.; Li, X.; Xing, J.; Yu, Z.; Yang, P.; Li, W.; Yu, W. Accurate Adjusting the Lattice Strain of Triple-Cation and Mixed-Halide Perovskites for High-Performance Photodetector. *ACS Appl. Mater. Interfaces* **2022**, *14* (24), 28154−28162.
(46) Liu, X.; Li, S.; Li, Z.; Cao, F.; Su, L.; Shtansky, D. V.; Fang, X. Enhanced Response Speed in 2D Perovskite Oxides-Based Photodetectors for UV Imaging through Surface/Interface Carrier-Transport Modulation. *ACS Appl. Mater. Interfaces* **2022**, *14* (43), 48936−48947.
(47) Yang, Y.; Peng, H.; Liu, C.; Arain, Z.; Ding, Y.; Ma, S.; Liu, X.; Hayat, T.; Alsaedi, A.; Dai, S. Bi-functional additive engineering for high-performance perovskite solar cells with reduced trap density. *J. Mater. Chem. A* **2019**, *7* (11), 6450−6458.
(48) Liu, C.; Cai, M.; Yang, Y.; Arain, Z.; Ding, Y.; Shi, X.; Shi, P.; Ma, S.; Hayat, T.; Alsaedi, A.; Wu, J.; Dai, S.; Cao, G. A C_{60}/TiO_x bilayer for conformal growth of perovskite films for UV stable perovskite solar cells. *J. Mater. Chem. A* **2019**, *7* (18), 11086−11094.
(49) Xie, C.; Mak, C.; Tao, X.; Yan, F. Photodetectors Based on Two-Dimensional Layered Materials Beyond Graphene. *Adv. Funct. Mater.* **2017**, *27* (19), 1603886.
(50) Qiu, J.; Zheng, Y.; Xia, Y.; Chao, L.; Chen, Y.; Huang, W. Rapid Crystallization for Efficient 2D Ruddlesden-Popper (2DRP) Perovskite Solar Cells. *Adv. Funct. Mater.* **2019**, *29* (47), 1806831.
(51) Fang, Y.; Dong, Q.; Shao, Y.; Yuan, Y.; Huang, J. Highly narrowband perovskite single-crystal photodetectors enabled by surface-charge recombination. *Nat. Photonics* **2015**, *9* (10), 679−686.
(52) Zai, H.; Ma, Y.; Chen, Q.; Zhou, H. Ion migration in halide perovskite solar cells: Mechanism, characterization, impact and suppression. *J. Energy Chem.* **2021**, *63*, 528−549.
(53) Lim, E. L.; Hagfeldt, A.; Bi, D. Toward highly efficient and stable Sn^{2+} and mixed Pb^{2+}/Sn^{2+} based halide perovskite solar cells through device engineering. *Energy Environ. Sci.* **2021**, *14* (6), 3256−3300.
(54) Yuan, Y.; Huang, J. Ion Migration in organometal trihalide perovskite and its impact on photovoltaic efficiency and stability. *Acc. Chem. Res.* **2016**, *49* (2), 286−293.
(55) Yang, W.-F.; Igbari, F.; Lou, Y.-H.; Wang, Z.-K.; Liao, L.-S. Tin halide perovskites: progress and challenges. *Adv. Energy Mater.* **2020**, *10* (13), 1902584.

https://doi.org/10.1021/acsaelm.3c00058
ACS Appl. Electron. Mater. 2023, 5, 2169−2177

(56) Huang, T.; Zhu, Z.; Zhao, C.; Kong, W.; Chen, X.; Li, R.; Yu, Z.; Shi, Z.; Li, D.; Yang, B.; Yu, W. Enhancing two-dimensional perovskite photodetector performance through balancing carrier density and directional transport. *J. Mater. Chem. A* **2022**, *10*, 21044−21052.

https://doi.org/10.1021/acsaelm.3c00058
ACS Appl. Electron. Mater. 2023, 5, 2169−2177